Polar vacuolar distribution is essential for accurate asymmetric division of *Arabidopsis* zygotes

Yusuke Kimata[a,1], Takehide Kato[b,1], Takumi Higaki[c,d], Daisuke Kurihara[a], Tomomi Yamada[a,e], Shoji Segami[f], Miyo Terao Morita[f,g], Masayoshi Maeshima[f], Seiichiro Hasezawa[c], Tetsuya Higashiyama[a,e], Masao Tasaka[b], and Minako Ueda[a,e,2]

[a]Division of Biological Science, Graduate School of Science, Nagoya University, Furo-cho, Chikusa-ku, Nagoya, 464-8602 Aichi, Japan; [b]Graduate School of Biological Sciences, Nara Institute of Science and Technology, Ikoma, 630-0192 Nara, Japan; [c]Department of Integrated Biosciences, Graduate School of Frontier Sciences, The University of Tokyo, Kashiwanoha, Kashiwa, 277-8562 Chiba, Japan; [d]International Research Organization for Advanced Science and Technology, Kumamoto University, Chuo-ku, 860-8555 Kumamoto, Japan; [e]Institute of Transformative Bio-Molecules, Nagoya University, Furo-cho, Chikusa-ku, Nagoya, 464-8601 Aichi, Japan; [f]Graduate School of Bioagricultural Sciences, Nagoya University, Nagoya, 464-8601 Aichi, Japan; and [g]National Institute for Basic Biology, Myodaiji, Okazaki, 444-8585 Aichi, Japan

Edited by Dominique C. Bergmann, Stanford University, Stanford, CA, and approved December 14, 2018 (received for review August 27, 2018)

In most flowering plants, the asymmetric cell division of the zygote is the initial step in establishing the apical–basal axis of the mature plant. The zygote is polarized, possessing the nucleus at the apical tip and large vacuoles at the basal end. Despite their known polar localization, whether the positioning of the vacuoles and the nucleus is coordinated and what the role of the vacuole is in the asymmetric zygotic division remain elusive. In the present study, we utilized a live-cell imaging system to visualize the dynamics of vacuoles during the entire process of zygote polarization in *Arabidopsis*. Image analysis revealed that the vacuoles formed tubular strands around the apically migrating nucleus. They gradually accumulated at the basal region and filled the space, resulting in asymmetric distribution in the mature zygote. To assess the role of vacuoles in the zygote, we screened various vacuole mutants and identified that *shoot gravitropism2* (*sgr2*), in which the vacuolar structural change was impaired, failed to form tubular vacuoles and to polarly distribute the vacuole. In *sgr2*, large vacuoles occupied the apical tip and thus nuclear migration was blocked, resulting in a more symmetric zygotic division. We further observed that tubular vacuole formation and asymmetric vacuolar distribution both depended on the longitudinal array of actin filaments. Overall, our results show that vacuolar dynamics is crucial not only for the polar distribution along actin filaments but also for adequate nuclear positioning, and consequently zygote-division asymmetry.

Arabidopsis thaliana | zygote | vacuole | apical–basal axis | live-cell imaging

Initiation of the main body axis is an incipient event required for a unicellular zygote to develop into a multicellular organism. In most flowering plants (both monocots and dicots), the apical–basal axis is formed along the longitudinal axis of the zygote marked by the nucleus in the apical region and large vacuoles in the basal region (1, 2). Large vacuoles are also observed in unfertilized egg cells but, after fertilization, the vacuoles are shrunk and/or dispersed into the entire cell (3–5). In the mature zygote, vacuoles are accumulated at the basal region and most vacuoles are inherited in the basal cell after asymmetric division of the zygote (1, 4, 5). Despite such obvious changes, the dynamics of vacuolar distribution and the role of vacuoles in the asymmetric zygotic division are unknown.

We recently developed a high-resolution live-cell imaging system utilizing an in vitro ovule cultivation method and two-photon excitation microscopy, and visualized the intracellular dynamics in *Arabidopsis* zygotes (6, 7). Using this system, we observed that actin filaments (F-actin) align longitudinally in the elongating zygote and are essential for apically directed nuclear migration (6). However, it remained unknown whether other organelles also distribute along F-actin and, if so, whether their positioning is coordinated or independent.

In this study, we performed live-cell imaging of vacuolar dynamics during zygote polarization. Various morphological features of the vacuoles were extensively compared at different zygotic stages in the wild type and the *shoot gravitropism2* (*sgr2*) mutant, which affects the vacuolar membrane protein, and after exposure to specific inhibitors for F-actin. We found that dynamic vacuolar distribution along F-actin is necessary for nuclear migration to the future division site. Our findings provide insights into the role of vacuoles in setting the accurate asymmetric division of the zygote in flowering plants.

Results

Vacuoles Form Thin Tubular Strands Around the Nucleus and Gradually Accumulate at the Basal Region During Zygote Elongation. To perform live-cell imaging of the vacuole in the polarizing zygote, we developed a dual-color marker that simultaneously labels the vacuolar membrane and nucleus (vacuole/nucleus) and could be imaged using two-photon excitation microscopy (2PEM) (Fig. 1 *A* and *B*). We detected the same pattern of polar localization for the vacuole and the nucleus as the fixed ovules of nontransgenic plants (Fig. 1 and *SI Appendix*, Fig. S1) (5), thus indicating that our system visualized native intracellular patterns.

We then captured the behavior using time-lapse imaging until the first zygotic cell division (Fig. 1 *B* and *C* and Movie S1). Before fertilization, the egg cell showed a clear polar organization, with the nucleus at the apical pole and huge vacuoles occupying the basal region. After fertilization, the cell shrunk as we previously reported (6), and vacuolar size was also markedly

Significance

The vacuole is one of the largest plant organelles. It occupies the basal region of the zygote and is mostly inherited in the basal daughter cell after zygotic division. In spite of the obvious asymmetry, how dynamically the vacuole is distributed and whether it contributes to apical–basal axis formation are unknown. In the present study, we report that the vacuole actively changes its shape and size and positions along actin filaments. We further show that vacuolar distribution supports nuclear localization at the opposite cell end, and thus ensures asymmetric division of the zygote. These results provide insights into cooperative organelle positioning during zygote polarization and the crucial roles of vacuoles in the initial steps of plant ontogeny.

Author contributions: Y.K., T.K., D.K., M.T.M., S.H., T. Higashiyama, M.T., and M.U. designed research; Y.K., T.K., T.Y., S.S., and M.U. performed research; Y.K., T. Higaki, and M.U. analyzed data; and Y.K., T. Higaki, D.K., M.T.M., M.M., and M.U. wrote the paper.

The authors declare no conflict of interest.

This article is a PNAS Direct Submission.

[1]Y.K. and T.K. contributed equally to this work.

[2]To whom correspondence should be addressed. Email: m-ueda@itbm.nagoya-u.ac.jp.

This article contains supporting information online at www.pnas.org/lookup/suppl/doi:10.1073/pnas.1814160116/-/DCSupplemental.

Published online January 16, 2019.

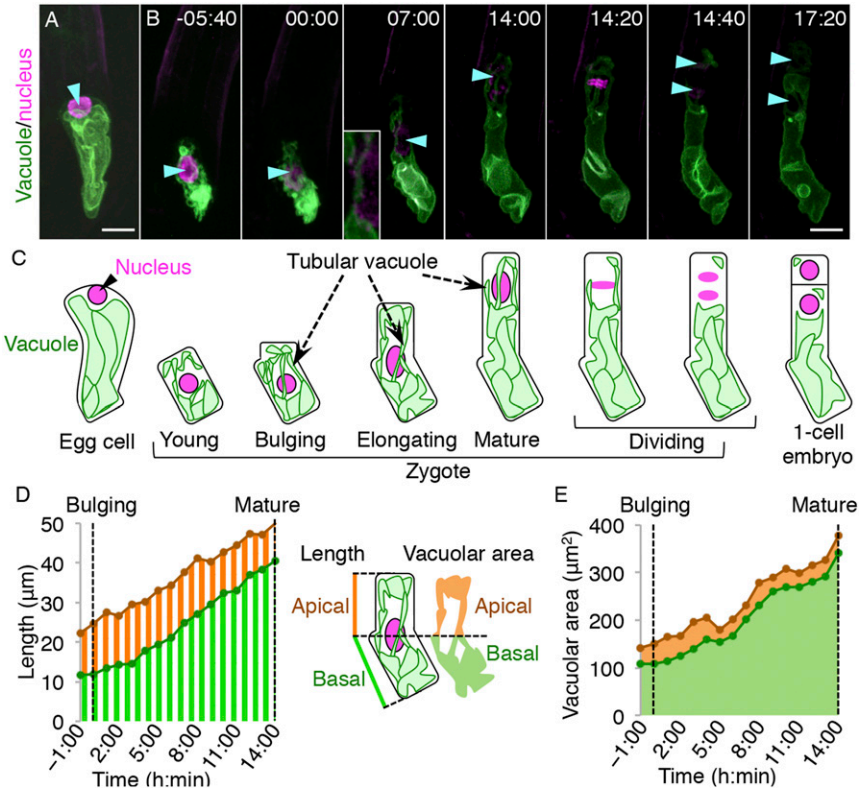

Fig. 1. Live-cell imaging and quantification of vacuolar dynamics during zygote polarization in wild type (WT). (*A* and *B*) 2PEM image of the egg cell (*A*) and time-lapse observation of the zygote in in vitro cultivated WT ovules (*B*) expressing the vacuolar/nuclear marker. Maximum-intensity projection (MIP) images are shown. Images are representative of 11 time-lapse images. Numbers indicate the time (h:min) from when the zygote started elongation ("bulging"). Cyan arrowheads indicate nuclei. (Scale bars, 10 μm.) (*B*, *Inset*) An enlarged image of the perinuclear region. (*C*) Illustrations showing a summary of the respective stages. (*D*) Time course of "apical" (orange stripe) and "basal" (green stripe) lengths, which are the distances from the center of the nucleus to the apical edge and the basal end of the cell, respectively, as shown (*Right*). Both lengths were measured from −1:00 until 14:00, when the zygote elongation was completed ("mature" zygote). (*E*) Time course of the apical (orange) and basal (green) vacuolar areas as shown in the illustration.

reduced. The nucleus shifted to the cell center, and the vacuoles were detected both in the apical and basal regions (Fig. 1 *D* and *E*). Then, the zygote elongated, and the vacuoles formed thin tubular structures around the nucleus, which migrates toward the apical tip (Fig. 1 *B*–*D*). Simultaneously, vacuolar size was also gradually increased. The vacuoles in the apical region remained small while vacuolar size in the basal area was massively increased, resulting in a highly asymmetric distribution of the vacuoles on completion of nuclear migration and zygotic elongation (Fig. 1 *B*, *C*, and *E*). Therefore, after chromosome segregation and cytokinesis, most of the vacuoles were inherited into the basal cell.

In summary, fertilization triggers vacuolar shrinkage, and the vacuoles swell again during zygote elongation. The nucleus becomes surrounded by thin vacuolar tubules and migrates to the apical apex, while the vacuoles gradually accumulate at the basal region.

The *sgr2-1* Mutant Is Defective in Asymmetrical Zygotic Division and Embryo Morphology. To understand the role of vacuoles in zygote polarization, we examined whether the zygote-division asymmetry was affected when vacuolar morphology and/or functions were disturbed. Because zygotic vacuolar regulators were not identified, we observed various vacuole mutants that exhibited defects in other tissues (*SI Appendix*, Fig. S1*A*). We found that *sgr2-1* zygotes divided in a more symmetrical manner (Fig. 2*A* and *SI Appendix*, Fig. S1*A*), as confirmed by the higher ratio of apical to basal daughter cell lengths than in the wild type (Fig. 2*B*). In contrast, the total lengths of one-cell-stage embryos were indistinguishable between the wild type and *sgr2-1* (Fig. 2*C*), indicating that cell elongation was unaffected in the *sgr2-1* zygote.

SGR2 (At1g31480) encodes a phospholipase A1-like protein localized on the vacuolar membrane (8, 9). Although the molecular function of SGR2 is still unknown, it has been reported that *sgr2-1* severely impairs the dynamic shape changes of vacuoles and thus generates spherical and less mobile vacuoles in inflorescence stems (10). Therefore, the sedimentable plastids (amyloplasts) that are surrounded by the vacuolar membrane cannot smoothly reposition in response to gravitational forces, resulting in reduced gravitropism (10). We noticed that in the unfertilized egg cell of *sgr2-1*, the huge vacuole normally located at the basal end with the nucleus at the apical top, although the precise vacuolar shape could not be distinguished in the fixed samples (*SI Appendix*, Fig. S1*B*). Large vacuoles were detected in the *sgr2-1* apical cell and also in the apical cell lineage (embryo proper) after zygotic division in all of the embryo stages examined, whereas only small vacuoles were detected in the wild type (Fig. 2 *A* and *D* and *SI Appendix*, Fig. S1 *A* and *B*). The *sgr2-1* embryos showed distorted shapes with aberrant cell-division planes (Fig. 2*D* and *SI Appendix*, Fig. S1 *A*–*C*), and the *sgr2-1* seedlings displayed morphological abnormalities such as the presence of three cotyledons (*SI Appendix*, Fig. S1*D*) (9). The *sgr2-1* phenotypes in the zygote and embryo were restored by the *SGR2* transgene (pSGR2::SGR2i-GFP), which complemented the gravitropic defects of *sgr2-1* (Fig. 2 *A*–*C* and *SI Appendix*, Fig. S1*A*) (8). These findings indicated that *SGR2* is required for proper vacuole distribution in the zygote, which would be important for zygote-division asymmetry and subsequent embryo development.

The *sgr2-1* Mutant Fails to Form Tubular Vacuoles and Has Disturbed Polar Vacuole Distribution and Nuclear Migration. We then performed time-lapse imaging of *sgr2-1* (Fig. 3 and Movie S2). As observed in the fixed samples, the *sgr2-1* egg cell polarly positioned the vacuole and the nucleus as in the wild type, although vacuoles were more spherical, as reported in inflorescence stems (Fig. 3*A*, compared with Fig. 1*A* and *SI Appendix*, Fig. S1*B*) (10). After fertilization, the *sgr2-1* zygote showed cell shrinkage, nuclear localization at the cell center, and dispersed vacuoles both in the apical and basal regions. The indistinguishable vacuolar features between *sgr2-1* and the wild type were confirmed by 3D reconstructed images (*SI Appendix*, Fig. S2*A*) and were also quantified by the similar values of circularity, perimeter, and area of the vacuole (Fig. 3 *G*–*I*), which were measured using a vacuolar lumen marker (*SI Appendix*, Fig. S2 *B* and *C*). However, during the zygotic elongation, *sgr2-1* did not form a tubular vacuole, and only spherical and spotted vacuoles were observed in the perinuclear region, as shown by the larger value of circularity than in the wild type (Fig. 3*G*). In addition, the

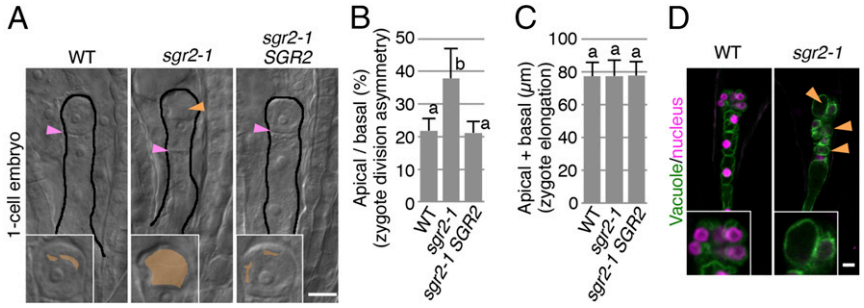

Fig. 2. Identification of the *sgr2-1* phenotypes in zygote-division asymmetry and embryo morphology. (*A*) DIC images of cleared one-cell-stage embryos of WT, *sgr2-1*, and *sgr2-1* containing the pSGR2::SGR2i-GFP transgene (*sgr2-1 SGR2*). Embryos are outlined, and the orange arrowhead indicates the apically remaining large vacuole, which is colored in the enlarged images (*Insets*). Magenta arrowheads indicate the cell-division planes. (*B*) The ratio of apical cells divided by basal cell lengths in one-cell-stage embryos, denoted as the asymmetric cell division of the zygote. (*C*) The total length of one-cell-stage embryos (sum of apical and basal cell lengths), denoted as zygote elongation. Error bars represent the SD ($N = 80$ for each genotype), and the letters indicate significant differences determined by Tukey–Kramer test; $P < 0.01$. (*D*) 2PEM images of eight-cell-stage embryos expressing the vacuolar/nuclear marker. Center plane images are shown. Orange arrowheads indicate the apically remaining large vacuoles, and *Insets* show the enlarged images of the apical region. (Scale bars, 10 μm.)

perimeter value in *sgr2-1* was smaller than in the wild type (Fig. 3*H*), indicating reduced vacuolar surface. The apical and basal vacuoles both gradually increased in size (Fig. 3*E*), and finally vacuolar distribution became more symmetric than in the wild type (Fig. 3*F*). In contrast to the abnormal vacuole shape and distribution, the total vacuole area was indistinguishable between the wild type and *sgr2-1* at all stages (Fig. 3 *F* and *I*), indicating that *sgr2-1* specifically affected the vacuole morphology and polar vacuole positioning without altering vacuole size. This, together with the observation that the vacuolar lumen marker did not show spotted vacuoles in *sgr2-1* (*SI Appendix*, Fig. S2*A*), suggested that SGR2 would be required to fuse small empty vacuoles with the large central vacuole, and thus to increase the vacuolar membrane component, not the vacuolar lumen volume.

The apical domain of the *sgr2-1* zygote was occupied by large spherical vacuoles (Fig. 3*E*), which prevented the nucleus from reaching the apical cell end (Fig. 3*D*). Even when the zygote completed cell elongation, the nucleus still remained near the cell center (Fig. 3*D*). Therefore, the *sgr2-1* zygote divided more symmetrically than that of the wild type, inheriting large vacuoles in the apical cell, which was consistent with the fixed-sample observations (Fig. 2 *A* and *B* and *SI Appendix*, Fig. S1 *A* and *B*). Despite the severe defect in cell-division asymmetry, cell-division timing was not affected in *sgr2-1*, as shown by the comparable time from the start of zygote elongation until the onset of nuclear division in the wild type (15 ± 5.6 h; $n = 11$) and in *sgr2-1* (15 ± 3.3 h; $n = 10$) [not significant ($P = 0.50$) by Mann–Whitney U test]. These results showed that SGR2 is crucial for the dynamic vacuolar shape change and polar vacuolar distribution, which support accurate nuclear positioning and thus zygote-division asymmetry.

Because the vacuole is a fundamental organelle in plants, we then examined whether the vacuole-dependent mechanism to regulate zygotic asymmetry works in other tissues. As typical events involving cell polarization and/or asymmetric cell division, we focused on root hair initiation at the basal end of epidermal cells (*SI Appendix*, Fig. S3*A*) (11), nuclear positioning in the root hair (*SI Appendix*, Fig. S3 *A* and *B*) (12), cell-layer formation in the root meristem (*SI Appendix*, Fig. S3*C*) (13), and stomatal shape and patterning (*SI Appendix*, Fig. S3*D*) (14). Although *SGR2* was expressed in whole seedlings (8) and the vacuole morphology was actually affected (*SI Appendix*, Fig. S3 *A* and *C*), we could not detect any defects in these processes in *sgr2-1*. These results suggested that the SGR2-dependent regulation of the asymmetric cell division is specific to the zygote.

Tubular Vacuole Formation and Polar Vacuole Distribution Depend on the Longitudinal Array of F-Actin. To identify the driving force of polar vacuole positioning, we tested the involvement of F-actin, because it is known to associate with vacuolar membranes and regulate vacuolar morphology during various cellular events, such as cell-cycle progression in tobacco culture cells (15) and cell elongation in *Arabidopsis* roots (16). We have recently reported that in the *Arabidopsis* zygote, the F-actin array is disorganized upon fertilization and then gradually aligns longitudinally along the apical–basal axis (Fig. 4 *A* and *B*, *SI Appendix*, Fig. S4 *A* and *B*, and Movie S3) (6), implying an analogy to the temporal shrinkage and tubular formation of vacuoles. As in the wild type, F-actin in the *sgr2-1* zygote was disorganized after fertilization and then gradually reorganized into parallel, dense, and thick bundles (*SI Appendix*, Fig. S4 *C*–*G* and Movie S4). Only the average angle of F-actin fibers ($\Delta\theta$) was not reduced in the mature zygote of *sgr2-1* (*SI Appendix*, Fig. S4*H*), indicating the less longitudinal alignment of F-actin cables in the whole cell. However, it seemed due to the large spherical vacuoles occupying the cell center in *sgr2-1* (Fig. 4*C*). Indeed, the F-actin was excluded from the spherical vacuoles in *sgr2-1* (Fig. 4*G*, *a*), whereas in the wild type the F-actin cable was detected in the basal vacuolar lumens, known as the transvacuolar strand. Moreover, the perinuclear F-actin was highly longitudinal and parallel both in the wild type and *sgr2-1* (Fig. 4 *B*, *D*, and *F*). In the perinuclear region, F-actin cables were associated with tubular vacuoles in the wild type but not in *sgr2-1* (Fig. 4*G*, *b*), showing that *sgr2-1* fails to form tubular vacuoles along F-actin.

We then used the actin polymerization inhibitor, latrunculin B (LatB), which effectively destroyed the F-actin pattern observed in our zygote imaging system (6). After a 3-h LatB treatment, the tubular vacuoles disappeared from the perinuclear region (Fig. 4 *H* and *I*). A similar disappearance of the perinuclear vacuoles was caused by another actin polymerization inhibitor, cytochalasin D (CytD), which also disrupted the F-actin pattern in the zygote (*SI Appendix*, Fig. S4*I*). Moreover, after a 24-h LatB treatment, the zygote divided in a more symmetric manner, generating highly vacuolated apical cells as in *sgr2-1* (Fig. 4 *J* and *K*). This LatB effect was not additive to *sgr2-1* (Fig. 4*K*), implying that the F-actin–dependent nuclear positioning is mainly due to the polar vacuole distribution.

Discussion

Our study demonstrated that vacuoles dynamically change in size, morphology, and position after fertilization (Fig. 4*L*). We further identified that the vacuolar membrane protein SGR2 and the longitudinal F-actin array are both necessary for polar vacuole distribution, which in turn supports nuclear migration and thus zygote-division asymmetry. Our findings provide evidence not only for the coordinated polar positioning of the vacuole and nucleus at opposite cell ends but also for the crucial role of the vacuole in cellular asymmetry in plant development.

After temporal shrinkage upon fertilization, the vacuole swells again, probably to help rapid zygote elongation without massive production of cytosol, as observed in other expanding cells (17). Zygote elongation was not affected in *sgr2-1*, which showed

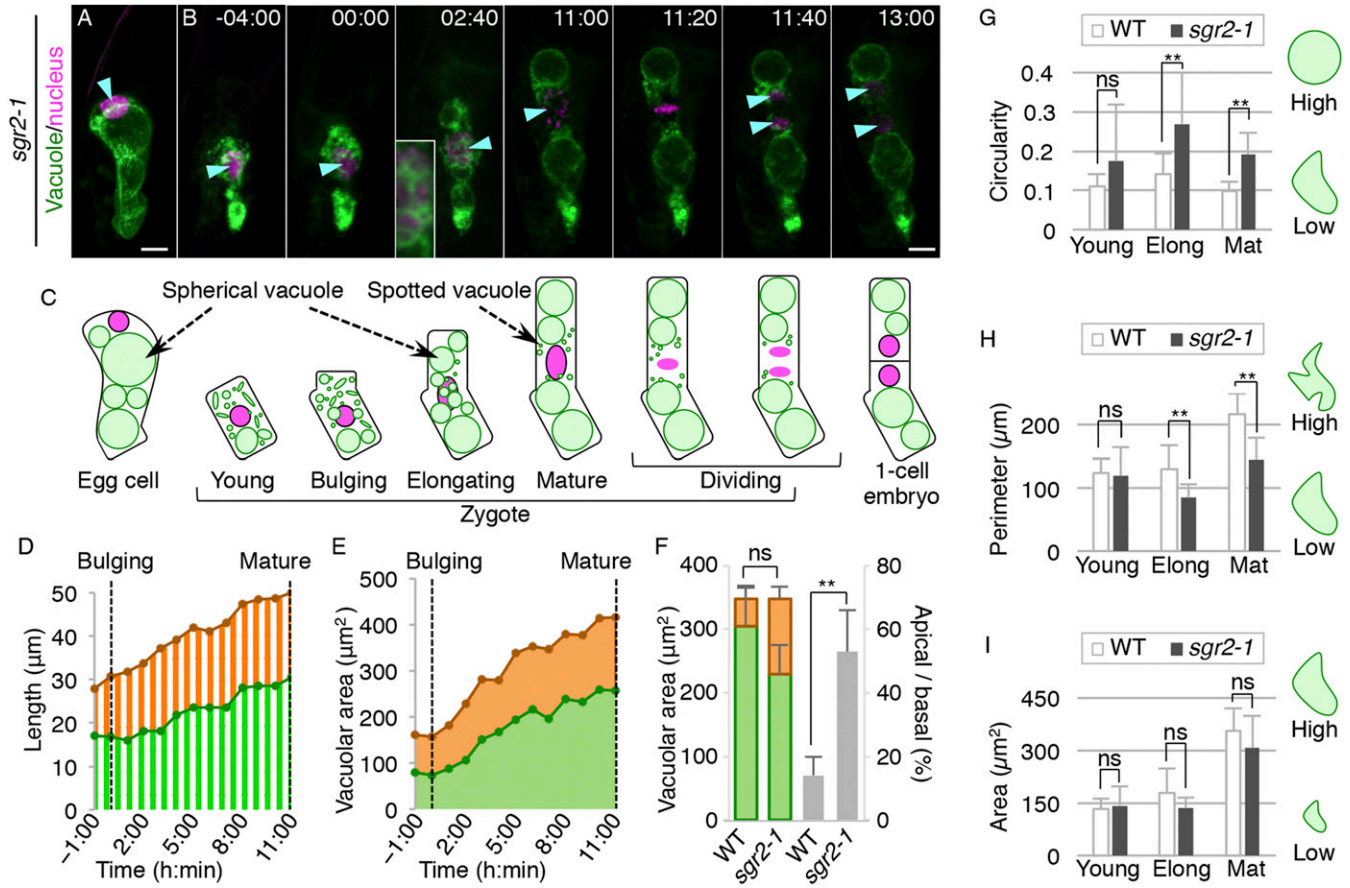

Fig. 3. Live-cell imaging and quantification of vacuolar dynamics during zygote polarization in *sgr2-1*. (*A* and *B*) 2PEM image of the egg cell (*A*) and time-lapse observation of the zygote in in vitro cultivated *sgr2-1* ovules (*B*) expressing the vacuolar/nuclear marker. MIP images are shown. Images are representative of 10 time-lapse images. Numbers indicate the time (h:min) from the bulging, and cyan arrowheads indicate the nuclei. (Scale bars, 10 μm.) (*B*, *Inset*) An enlarged image of the perinuclear region. (*C*) Illustrations showing a summary of the respective stages. (*D* and *E*) Time course of the lengths and vacuolar areas in apical and basal regions, as in Fig. 1 *D* and *E*, respectively. Both values were measured from −1:00 until 11:00, when the zygotic elongation was completed. (*F*) Graph of the sum of apical (orange) and basal (green) vacuolar areas (*Left*) in the mature zygotes, denoted as total vacuole size, and the ratio of the apical area divided by the basal vacuolar area (gray; *Right*), denoted as asymmetric vacuole distribution. Error bars represent the SD [$N = 11$ (WT) and 10 (*sgr2-1*)], and significant differences from the WT values were determined by Mann–Whitney *U* test; $^{**}P < 0.01$; ns, not significant. (*G–I*) Graphs of the circularity (*G*), perimeter (*H*), and area (*I*) of the vacuolar region at the indicated stages. Elong, elongating zygote; Mat, mature zygote. Error bars represent the SD [$N = 14$ (WT, Young), 12 (*sgr2-1*, Young), 14 (WT, Elong), 8 (*sgr2-1*, Elong), 17 (WT, Mat), and 13 (*sgr2-1*, Mat)], and significant differences from the values of the WT were determined by Brunner–Munzel test; $^{**}P < 0.01$. (*G–I*, *Right*) Illustrations show the correlation between the vacuolar features and the respective values.

proper vacuole size changes, but vacuole positioning was severely impaired. These results indicate different genetic requirements for the vacuole volume change and the polar vacuole distribution. Polar vacuole distribution would be specific for particular aspects, such as zygote polarization and gravity sensing, in which dynamic vacuolar shape change and coordinated organelle positioning occur synchronously (18). This specificity is supported by the observations that *sgr2-1* did not affect asymmetric cell division in roots and stomata, and various vacuole mutants did not disturb zygote-division asymmetry. Furthermore, the roles of F-actin in the zygote and other elongating cells might also be different, because F-actin regulates vacuole occupancy for root cell growth and thus LatB treatment inhibits root elongation (16), whereas in the zygote, LatB rarely impairs zygote elongation (6) but severely blocks polar vacuole distribution.

We also showed that in *sgr2-1*, nuclear migration was blocked by the large vacuoles occupying the apical region. Therefore, proper vacuole distribution is necessary for the nucleus to reach the appropriate apical site, probably via making free apical space for the nucleus (Fig. 4*L*). Their cooperative positioning is required not only for accurate asymmetrical zygotic division but also for the unequal inheritance of the vacuole into two daughter cells. This would ensure proper embryo development, possibly by generating a cytoplasmic apical cell to produce the highly proliferating embryo proper and a vacuolated basal cell to produce the rapidly elongating extraembryonic suspensor (Fig. 4*L*). Indeed, excess vacuoles in the embryo proper cause distorted embryo shape in the *sgr8*/*gravitropism defective2* mutant (19), and reduced vacuoles in the suspensor also disturb embryo patterning in *vacuoleless* (20).

To explain the mechanism underlying polar vacuole distribution in the zygote, the simple hypotheses would be predominant vacuole biogenesis at the basal region and/or directional vacuole migration along F-actin. Although the latter idea would be supported by the observation of tubular vacuoles associating with F-actin, our current knowledge of vacuole dynamics is too poor to determine the mechanism (17). Therefore, future investigations like live imaging of various vesicle trafficking routes for vacuole biogenesis, such as the adaptor protein complex 3-mediated pathway (17, 21), and the identification of the factors that link vacuoles to F-actin, such as myosin motor proteins (22), are warranted. These findings would also help to understand how SGR2 contributes to polar vacuole distribution. The *sgr2-1* zygote harbored many spotted vacuoles and reduced the vacuolar perimeter, suggesting that SGR2 is required to fuse small vacuoles with the large central vacuole, thereby increasing the

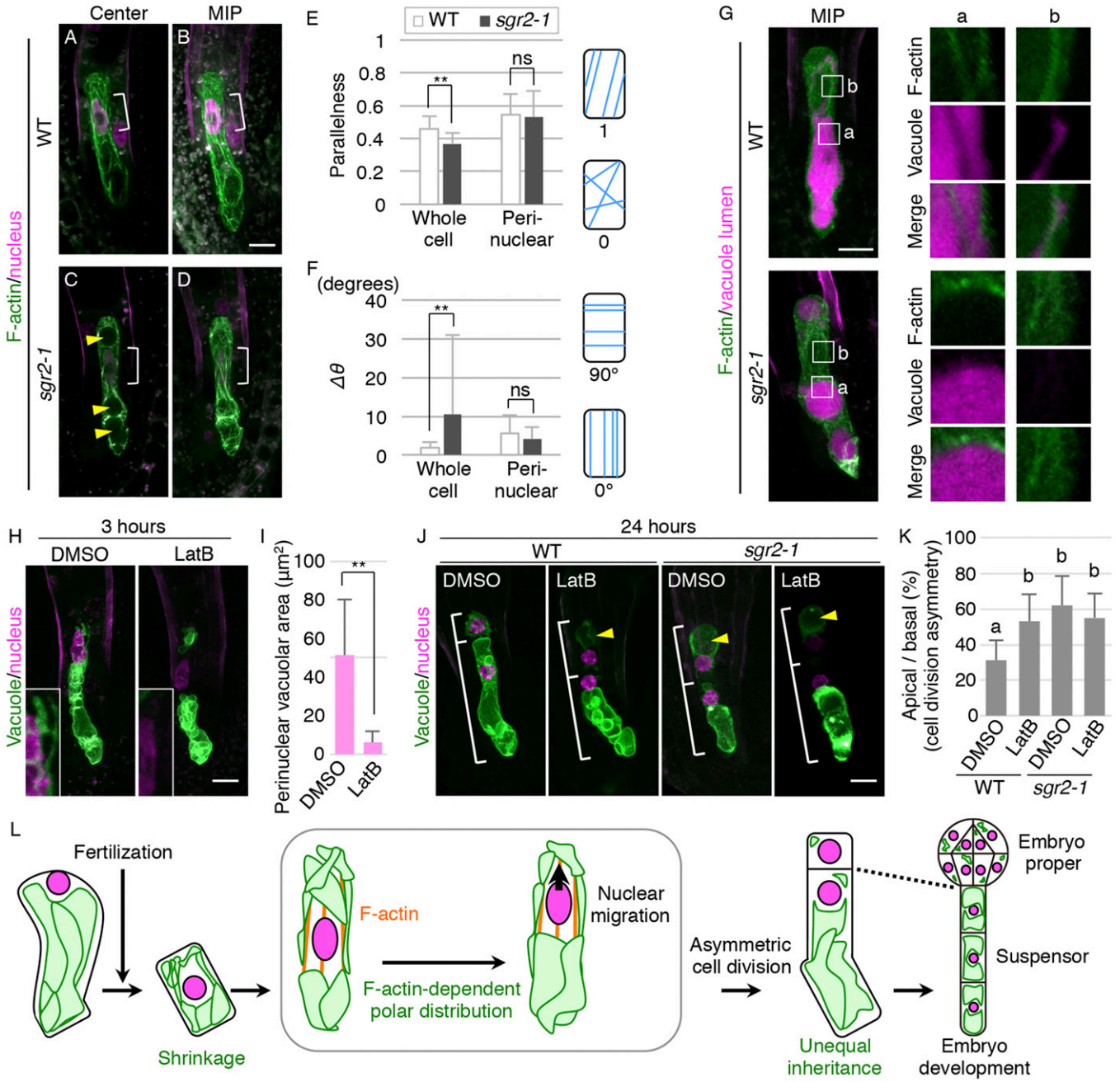

Fig. 4. Pattern and role of F-actin cables in tubular vacuole formation and polar vacuole positioning. (*A*–*D*) 2PEM images of mature zygotes expressing the F-actin/nuclear marker. Center plane (*A* and *C*) and MIP images (*B* and *D*) are shown. Yellow arrowheads indicate large spherical vacuoles, and brackets indicate the perinuclear regions. (*E* and *F*) Graphs of the parallelness (*E*) and average angle of the fibers against the cell longitudinal axis ($\Delta\theta$; *F*) of F-actin in the indicated cell areas of mature zygotes. Error bars represent the SD [$N = 12$ (WT) and 13 (*sgr2-1*)], and significant differences from WT values were determined by Brunner–Munzel test; $^{**}P < 0.01$; ns, not significant. Average values in the whole-cell area were significantly different between WT and *sgr2-1*, but values in the perinuclear region between the apical edge and the basal end of the nucleus were similar in WT and *sgr2-1*. Illustrations show the correlation between the respective values and the fiber patterns. (*G*) 2PEM images of mature zygotes expressing the F-actin/vacuolar lumen marker. Magnified images of the square areas (*a* and *b*) are shown (*Right*). MIP images are shown for the whole-cell area, and single z slices are shown in the magnified area. Images are representative of five and seven samples for WT and *sgr2*, respectively. (*G*, *a*) The transvacuolar strand in the basal vacuoles of WT, which did not appear in *sgr2-1*. (*G*, *b*) The association of tubular vacuoles with F-actin cables in WT, and the lack of detectable perinuclear vacuoles in *sgr2-1*. (*H*) 2PEM images of mature zygotes expressing the vacuolar/nuclear marker after exposure to the control DMSO and the polymerization inhibitor of F-actin (1 μM LatB) for 3 h. (*H*, *Insets*) Enlarged images of the perinuclear region. (*I*) Graph of the vacuolar area in the perinuclear region of DMSO- and LatB-treated zygotes for 3 h. Error bars represent the SD [$N = 9$ (WT) and 7 (*sgr2-1*)], and significant differences from the values of the DMSO-treated zygotes were determined by two-sided Welch's *t* test; $^{**}P < 0.01$. (*J*) 2PEM images of one-cell-stage embryos of WT and *sgr2-1* expressing the vacuolar/nuclear marker after exposure to DMSO and LatB for 24 h. Yellow arrowheads indicate the large vacuoles in the apical cells, and brackets indicate the lengths of the apical and basal cells. (*K*) The ratio of apical cells divided by basal cell lengths in one-cell-stage embryos of DMSO- and LatB-treated zygotes for 24 h. Error bars represent the SD [$N = 9$ (WT, DMSO), 10 (WT, LatB), 10 (*sgr2-1*, DMSO), and 9 (*sgr2-1*, LatB)], and letters indicate significant differences determined by Tukey–Kramer test; $P < 0.05$. (*L*) Schematic representation of the dynamics and roles of vacuoles and F-actin in zygote polarization and embryo development. (Scale bars, 10 μm.)

amount of vacuolar membrane. It is easy to imagine that the abundant vacuolar surface is necessary for flexible shape change, and thus insufficient vacuolar membrane would cause rigid and spherical vacuoles as found in *sgr2-1*. This, taken together with the fact that *SGR2* encodes a phospholipase A1-like protein localized on the vacuolar membrane (8), shows SGR2 might be important to degrade and/or produce some specific phospholipids, which regulate vacuolar membrane fusion. Previous studies have shown that vacuolar organization is controlled by various phospholipids, such as phosphatidylinositol 3,5-bisphosphate and phosphatidylinositol 3-phosphate (PI3P) (23–25). In particular, pharmacological depletion of PI3P rescues the vacuolar defects of the *vesicle transport through interaction with t-snares11* (*vti11*) mutant of vacuolar/PVC Qb-SNARE, which regulates vacuolar membrane fusion (26–28), showing the negative effect of PI3P on vacuolar fusion. Mutants in *vti11* produce spherical vacuoles and show impaired gravitropic response (9, 29), implying an analogy to *sgr2-1*. Therefore, SGR2 might similarly contribute to increasing vacuolar surface and thus indirectly assist flexible vacuolar shape change along F-actin. However, we cannot exclude the possibility that SGR2 supports the interaction of the vacuole and F-actin in a more direct manner, because several phospholipids are known to bind to F-actin–associating factors, such as myosin and actin-binding proteins in animal cells (30, 31). Future studies, such as the identification of enzymatic targets of SGR2 and live imaging of various phospholipids during zygote polarization (32), will demonstrate how SGR2 regulates vacuolar dynamics in the zygote.

Materials and Methods

Detailed materials and methods are described in *SI Appendix*.

Strains and Growth Conditions. All *Arabidopsis* lines were in the Columbia (Col-0) background, and *sgr2-1* has been described previously (9). The complemented *sgr2-1* by pSGR2::SGR2i-GFP was described previously (8). Plants were grown at 18 to 22 °C under continuous light or long-day conditions (16-h light/8-h dark).

Plasmid Construction. The vacuolar marker for the egg cell and the zygote was EC1p::VHP1-mGFP, consisting of the EGG CELL1 (EC1) promoter (33), monomeric GFP (mGFP), and VACUOLAR H^+-PPASE (VHP1) (34). The vacuolar lumen marker was EC1p::SP-mTur2-CTPP, containing the signal peptide (SP), mTurquoise2 (mTur2), and the vacuolar sorting signal COOH-terminal propeptide (CTPP) (35). Details of cloning procedures are shown in *SI Appendix*.

Zygote Imaging and Inhibitor Treatment. In vitro ovule culturing and 2PEM live-cell imaging were performed as previously described (6, 7). For the inhibitor treatment, 0.1% DMSO and 1 μM LatB (Sigma) and 100 μM CytD (Sigma) dissolved in 0.1% DMSO were added to the ovule cultivation media as previously described (6). An AxioImager A2 (Zeiss) was used for differential interference contrast (DIC) microscopy.

Quantitative Analysis of Vacuoles and F-Actin Structures. Image processing and measurements of lengths and vacuolar areas were performed using the binarized maximum-intensity projection images of vacuolar/nuclear markers with ImageJ software (https://imagej.nih.gov/ij/index.html). ImageJ was also used to quantify the circularity, perimeter, and area of the vacuolar lumen marker. The quantification of F-actin pattern was performed as previously described (6).

ACKNOWLEDGMENTS. We thank Hanae Tsuchiya, Yumi Kuwabara, and Yuriko Toda for technical support; Daisuke Maruyama for providing the vacuolar lumen reporter; and Kazuo Ebine and Takashi Ueda for providing the *sand-2* mutant. This work was supported by the Japan Society for the Promotion of Science: Grant-in-Aid for JSPS Research Fellow (JP18J10512 to Y.K.), Grants-in-Aid for Scientific Research on Innovative Areas [JP15H05962, JP15H05955, and JP17H05838 to M.U.; JP16H06465, JP16H06464, and JP16K21727 to T. Higashiyama; JP24114007 to S.H.; JP16H01235 to M.M.; and JP16H06280 (Advanced Bioimaging Support)], Grants-in-Aid for Young Scientists (A, JP25711017 to T. Higaki; and B, JP16K18687 to S.S.), Grants-in-Aid for Scientific Research (B, JP16H04802 to S.H.; JP17H03697 to D.K.; and A, JP26252011 to M.M.), Grants-in-Aid for Challenging Exploratory Research (JP16K14753 to M.U.; and JP17K19380 to T. Higaki), Grant-in-Aid for Scientific Research on Priority Areas (JP16085205 to M.T.M.), and PRESTO Project, Japan Science and Technology Agency (M.T.M.).

1. Mansfield SG, Briarty LG (1991) Early embryogenesis in *Arabidopsis thaliana*. II. The developing embryo. *Can J Bot* 69:461–476.
2. Suzuki K, Taniguchi T, Maeda E (1992) Ultrastructure and cleavage pattern of rice proembryos. *Jpn J Sci* 61:292–303.
3. Faure JE, Rotman N, Fortuné P, Dumas C (2002) Fertilization in *Arabidopsis thaliana* wild type: Developmental stages and time course. *Plant J* 30:481–488.
4. Jensen WA (1968) Cotton embryogenesis: The zygote. *Planta* 79:346–366.
5. Ueda M, Zhang Z, Laux T (2011) Transcriptional activation of *Arabidopsis* axis patterning genes *WOX8/9* links zygote polarity to embryo development. *Dev Cell* 20: 264–270.
6. Kimata Y, et al. (2016) Cytoskeleton dynamics control the first asymmetric cell division in *Arabidopsis* zygote. *Proc Natl Acad Sci USA* 113:14157–14162.
7. Kurihara D, Kimata Y, Higashiyama T, Ueda M (2017) In vitro ovule cultivation for live-cell imaging of zygote polarization and embryo patterning in *Arabidopsis thaliana*. *J Vis Exp*, 10.3791/55975.
8. Morita MT, et al. (2002) Involvement of the vacuoles of the endodermis in the early process of shoot gravitropism in *Arabidopsis*. *Plant Cell* 14:47–56.
9. Kato T, et al. (2002) SGR2, a phospholipase-like protein, and ZIG/SGR4, a SNARE, are involved in the shoot gravitropism of *Arabidopsis*. *Plant Cell* 14:33–46.
10. Toyota M, et al. (2013) Amyloplast displacement is necessary for gravisensing in *Arabidopsis* shoots as revealed by a centrifuge microscope. *Plant J* 76:648–660.
11. Fischer U, Ikeda Y, Grebe M (2007) Planar polarity of root hair positioning in *Arabidopsis*. *Biochem Soc Trans* 35:149–151.
12. Chytilova E, et al. (2000) Nuclear dynamics in *Arabidopsis thaliana*. *Mol Biol Cell* 11: 2733–2741.
13. Van Norman JM (2016) Asymmetry and cell polarity in root development. *Dev Biol* 419:165–174.
14. Facette MR, Smith LG (2012) Division polarity in developing stomata. *Curr Opin Plant Biol* 15:585–592.
15. Higaki T, Kutsuna N, Okubo E, Sano T, Hasezawa S (2006) Actin microfilaments regulate vacuolar structures and dynamics: Dual observation of actin microfilaments and vacuolar membrane in living tobacco BY-2 cells. *Plant Cell Physiol* 47:839–852.
16. Scheuring D, et al. (2016) Actin-dependent vacuolar occupancy of the cell determines auxin-induced growth repression. *Proc Natl Acad Sci USA* 113:452–457.
17. Krüger F, Schumacher K (2018) Pumping up the volume—Vacuole biogenesis in *Arabidopsis thaliana*. *Semin Cell Dev Biol* 80:106–112.
18. Singh M, Gupta A, Laxmi A (2017) Striking the right chord: Signaling enigma during root gravitropism. *Front Plant Sci* 8:1304.
19. Silady RA, et al. (2008) The GRV2/RME-8 protein of *Arabidopsis* functions in the late endocytic pathway and is required for vacuolar membrane flow. *Plant J* 53:29–41.
20. Rojo E, Gillmor CS, Kovaleva V, Somerville CR, Raikhel NV (2001) VACUOLELESS1 is an essential gene required for vacuole formation and morphogenesis in *Arabidopsis*. *Dev Cell* 1:303–310.
21. Feraru E, et al. (2010) The AP-3 β adaptin mediates the biogenesis and function of lytic vacuoles in *Arabidopsis*. *Plant Cell* 22:2812–2824.
22. Avisar D, et al. (2009) A comparative study of the involvement of 17 *Arabidopsis* myosin family members on the motility of Golgi and other organelles. *Plant Physiol* 150:700–709.
23. Whitley P, Hinz S, Doughty J (2009) *Arabidopsis* FAB1/PIKfyve proteins are essential for development of viable pollen. *Plant Physiol* 151:1812–1822.
24. Nováková P, et al. (2014) SAC phosphoinositide phosphatases at the tonoplast mediate vacuolar function in *Arabidopsis*. *Proc Natl Acad Sci USA* 111:2818–2823.
25. Lee Y, et al. (2008) The *Arabidopsis* phosphatidylinositol 3-kinase is important for pollen development. *Plant Physiol* 147:1886–1897.
26. Ebine K, et al. (2014) Plant vacuolar trafficking occurs through distinctly regulated pathways. *Curr Biol* 24:1375–1382.
27. Sanderfoot AA, Kovaleva V, Bassham DC, Raikhel NV (2001) Interactions between syntaxins identify at least five SNARE complexes within the Golgi/prevacuolar system of the *Arabidopsis* cell. *Mol Biol Cell* 12:3733–3743.
28. Zheng J, Han SW, Rodriguez-Welsh MF, Rojas-Pierce M (2014) Homotypic vacuole fusion requires VTI11 and is regulated by phosphoinositides. *Mol Plant* 7:1026–1040.
29. Saito C, et al. (2011) The occurrence of 'bulbs', a complex configuration of the vacuolar membrane, is affected by mutations of vacuolar SNARE and phospholipase in *Arabidopsis*. *Plant J* 68:64–73.
30. Senju Y, et al. (2017) Mechanistic principles underlying regulation of the actin cytoskeleton by phosphoinositides. *Proc Natl Acad Sci USA* 114:E8977–E8986.
31. Liu X, et al. (2016) Mammalian nonmuscle myosin II binds to anionic phospholipids with concomitant dissociation of the regulatory light chain. *J Biol Chem* 291: 24828–24837.
32. Simon ML, et al. (2014) A multi-colour/multi-affinity marker set to visualize phosphoinositide dynamics in *Arabidopsis*. *Plant J* 77:322–337.
33. Sprunck S, et al. (2012) Egg cell-secreted EC1 triggers sperm cell activation during double fertilization. *Science* 338:1093–1097.
34. Segami S, Makino S, Miyake A, Asaoka M, Maeshima M (2014) Dynamics of vacuoles and H^+-pyrophosphatase visualized by monomeric green fluorescent protein in *Arabidopsis*: Artifactual bulbs and native intravacuolar spherical structures. *Plant Cell* 26:3416–3434.
35. Vitale A, Raikhel NV (1999) What do proteins need to reach different vacuoles? *Trends Plant Sci* 4:149–155.